Electrochemistry

International Edition: DOI: 10.1002/anie.201605102
German Edition: DOI: 10.1002/ange.201605102

Cation Intercalation in Manganese Oxide Nanosheets: Effects on Lithium and Sodium Storage

Ke Lu, Ziyu Hu, Zhonghua Xiang, Jizhen Ma, Bin Song, Jintao Zhang, and Houyi Ma**

Abstract: *The rapid development of advanced energy-storage devices requires significant improvements of the electrode performance and a detailed understanding of the fundamental energy-storage processes. In this work, the self-assembly of two-dimensional manganese oxide nanosheets with various metal cations is introduced as a general and effective method for the incorporation of different guest cations and the formation of sandwich structures with tunable interlayer distances, leading to the formation of 3D M_xMnO_2 ($M = Li$, Na, K, Co, and Mg) cathodes. For sodium and lithium storage, these electrode materials exhibited different capacities and cycling stabilities. The efficiency of the storage process is influenced not only by the interlayer spacing but also by the interaction between the host cations and shutter ions, confirming the crucial role of the cations. These results provide promising ideas for the rational design of advanced electrodes for Li and Na storage.*

Two-dimensional (2D) metal oxide nanosheets (e.g., MnO_2, Co_3O_4, TiO_2, WO_3) with high surface-to-volume ratios often exhibit unique physicochemical properties, which have led to worldwide research interest in their application in transistors, energy-storage devices, and electrocatalysis.[1] For energy-storage applications, layered transition metal oxides (MO_2; M = Ti, V, Cr, Mn) have been intensively investigated as promising electrode materials for Li storage and recently also for Na storage along with the increasing interest in Na ion batteries (NIBs).[1b,2] During the charge–discharge process, the insertion/extraction of Li or Na ions often results in variations in the layer distances, which is accompanied by successive phase transitions.[2] A recent study revealed that the removal of alkali metal ions (e.g., Na^+) from layered Na_xCrO_2 led to the transformation of the layered structure into a rock salt structure.[2c] As a result, the layered structure collapsed, which eventually led to severe capacity decay. This study highlighted the crucial role of cations for energy storage in layered metal oxides. Such phase transitions and the structural changes in transition metal oxide layers (e.g., Na_xMnO_2) can be minimized by substitution/doping with electrochemically inactive elements (e.g., Ni, Mg), which results in stable 2D frameworks with good capacity retention.[3] However, it is still difficult to construct layered cathodes with adjustable ion channels for both Li and Na ion intercalation. In particular, the effect of different interlayer cations on the storage capacity and cycling stability of layered metal oxides has not been investigated thus far.

As interesting building blocks, 2D metal oxide nanosheets provide ideal platforms to adjust the microstructures and properties of such materials.[1c,4] For example, the wet spinning of 2D titania sheets generates macroscopic titania fibers with good mechanical properties through the alignment of stacked sheets with enhanced sheet-to-sheet binding interactions.[1c] Manganese dioxides possess various remarkable features, such as a high theoretical capacity (ca. 1232 $mAh\,g^{-1}$ as an anode), structural diversity (e.g., tunnels, layers), natural abundance, and environmental friendliness, and have been extensively studied as electrode materials for batteries and supercapacitors.[5] However, the use of MnO_2 as a cathode material for both Li ion batteries (LIBs) and NIBs has been hardly studied owing to its intrinsically low electrical conductivity, lack of suitable ion intercalation channels, and rapid capacity fading.[6] However, 2D manganese oxide nanosheets with molecular thickness provide a great opportunity for modulating the microstructure to enhance the energy storage capability through interface engineering and the integration of 2D nanosheets into three-dimensional (3D) porous frameworks.[5c,7] Unfortunately, the reported methods are often limited by multistep exfoliation and reassembly processes.[7a,8]

Herein, a bottom-up strategy has been developed to fabricate hierarchically sandwiched frameworks composed of manganese oxide nanosheets and various guest metal cations (e.g., Li^+, Na^+, K^+, Co^{2+}, and Mg^{2+}).[9] Owing to their polyelectrolytic and colloidal nature, the layer-by-layer self-assembly of manganese oxide nanosheets with cations leads to the formation of porous frameworks (Scheme 1).[7a,10] In particular, owing to the exchangeable guest cations, the interlayer spacings between the manganese oxide nanosheets can be adjusted. The electrochemical properties of the resultant manganese oxides and their ability for Li and Na

[*] K. Lu, J. Ma, Prof. J. Zhang, Prof. H. Ma
Key Laboratory for Colloid and Interface Chemistry of State Education Ministry, School of Chemistry and Chemical Engineering
Shandong University, Jinan 250100 (China)
E-mail: jtzhang@sdu.edu.cn
hyma@sdu.edu.cn
Dr. Z. Hu
Beijing Computational Science Research Center
No.10 East Xibeiwang Road, Haidian District, Beijing 100193 (China)
Prof. Z. Xiang
State Key Laboratory of Organic-Inorganic Composites
Beijing University of Chemical Technology
Beijing 100029 (China)
B. Song
Jiangsu Key Laboratory for Carbon-Based Functional Materials and Devices, Institute of Functional Nano and Soft Materials (FUNSOM)
Soochow University, Suzhou 215123 (China)
Supporting information and the ORCID identification numbers for the authors of this article can be found under http://dx.doi.org/10.1002/anie.201605102.

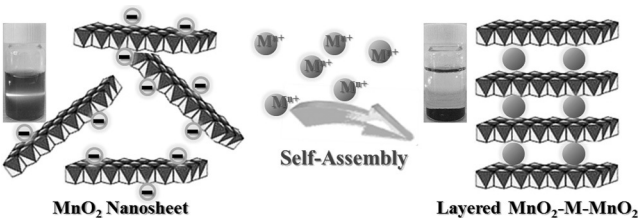

Scheme 1. Preparation of 3D layered manganese oxide frameworks.

storage were investigated to clarify the effect of the cation on their storage abilities and stabilities. These layered manganese oxide electrodes indeed showed good electrochemical performance for both Li and Na storage. Our experiments revealed that the capacities and stabilities of the electrode materials are influenced by both the cation size and their interaction with the shutter ions (Li^+ or Na^+), demonstrating the crucial role of the cations. These fundamental findings provide significant information for the rational design of suitable host materials with fast sodiation/desodiation (lithiation/delithiation) kinetics.

A colloidal suspension of manganese oxide nanosheets was obtained by rapid oxidation of Mn^{2+} ions in the presence of tetraethylammonium hydroxide (TMA·OH).[9] The obtained manganese oxide nanosheets are composed of edge-sharing MnO_6 octahedra in which some of the Mn^{4+} ions have been replaced by Mn^{3+} ions, which leads to a net negative charge, giving a colloidal suspension owing to the electrostatic repulsion. The nanosheet dispersion was purified by dialysis to remove residual TMA·OH. The obvious Tyndall effect suggests the formation of well-dispersed manganese oxide colloids. The neutralization of surface charges with metal cations leads to the electrostatic precipitation of manganese oxide nanosheets by layer-by-layer self-assembly (Scheme 1). As a result, 3D sandwiched manganese oxide frameworks were obtained that consist of repeating 2D host oxide layers that are separated by the guest cations.

The well-dispersed manganese oxide colloids with obvious light scattering owing to the Tyndall effect are shown in Figure 1 a. The addition of various cations (i.e., Li^+, Na^+, K^+, Mg^{2+}, and Co^{2+}) led to the electrostatic co-precipitation of the manganese oxide nanosheets with the metal cations. The chemical compositions of the samples were determined by inductively coupled plasma atomic emission spectroscopy (ICP-AES; see the Supporting Information, Table S1). Hereafter, the manganese oxides co-precipitated with Li^+, Na^+, K^+, Mg^{2+}, and Co^{2+} (M_xMnO_2) will be refereed to as LiMO, NaMO, KMO, MgMO, CoMO, respectively. The theoretical results (see the Supporting Information, Figure S1) reveal that the interlayer spacing increases with an increase in the diameter of the added cation (i.e., Li^+, Na^+, K^+, and Co^{2+}). The presence of (001) diffraction peaks in the powder X-ray diffraction (XRD) patterns (Figure 1 b) suggests that the manganese oxide nanosheets are uniformly stacked in the birnessite phase with interlayered cations.[9] A gradual peak shift from about 12° for LiMO to approximately 9° for MgMO was observed, indicating that the interlayer space was enlarged by the insertion of guest cations with larger

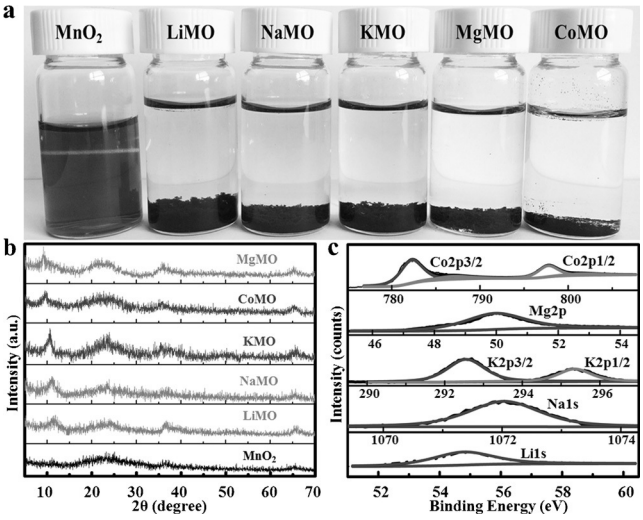

Figure 1. a) Digital photographs of the manganese oxide colloidal suspension and various M_xMnO_2 samples. b) XRD patterns of manganese oxide and M_xMnO_2. c) High-resolution XPS spectra showing the Li 1s, Na 1s, K 2p, Mg 2p, and Co 2p peaks for M_xMnO_2.

diameters.[4a,11] The interlayer distances calculated from the (001) peaks of LiMO, NaMO, KMO, CoMO, and MgMO are approximately 6.7, 7.1, 7.4, 7.8, and 7.9 Å according to the Bragg equation.[12] Hydration of the cations may result in the larger interlayer distances during the self-assembly process. Therefore, the interlayer distance can be easily adjusted by the intercalation of different guest cations during the co-precipitation process. To enhance the storage ability, lithiation and oxidation have recently been used to exfoliate and reassemble layered metal oxides and sulfides (e.g., $LiCoO_2$, MoS_2).[8b,c] This complex multistep process can be simplified by directly synthesizing manganese oxide nanosheets. More importantly, the simple self-assembly during the co-precipitation process directly produces manganese oxide nanosheets separated by the desired cations, providing an efficient approach to adjusting the layer stacking distance. With the resultant electrode materials, the effect of the various cations on Li^+ and Na^+ storage can be investigated.

The X-ray photoelectron spectra (XPS) of manganese dioxide nanosheets and M_xMnO_2 samples feature two peaks located at 642.0 and 653.9 eV, which were ascribed to Mn $2p_{3/2}$ and Mn $2p_{1/2}$ of Mn^{IV} (Figure S2), suggesting the formation of manganese dioxide.[9] The XPS peaks of Li 1s (54.9 eV), Na 1s (1072.0 eV), K 2p (292.6 and 295.3 eV), Mg 2p (50.0 eV), and Co 2p (782.5 and 797.6 eV; Figure 1 c) confirm the successful incorporation of these cations into the self-assembled frameworks. The absorption band in the Fourier transform infrared (FTIR) spectrum at 510 cm^{-1} was ascribed to the Mn–O vibrations of the as-prepared manganese oxide nanosheets and M_xMnO_2 samples(Figure S3).

For the manganese oxide nanosheets, transmission electron microscopy (TEM) and atomic force microscopy (AFM) images reveal the high 2D anisotropy with a lateral dimension in the sub-micrometer range (Figure 2 a) and a thickness of approximately 0.8 nm (Figure 2 b). Figure 2 c shows the crumpled structure of NaMO with many wrinkles and folds, whereas a crystalline structure is formed in the presence of

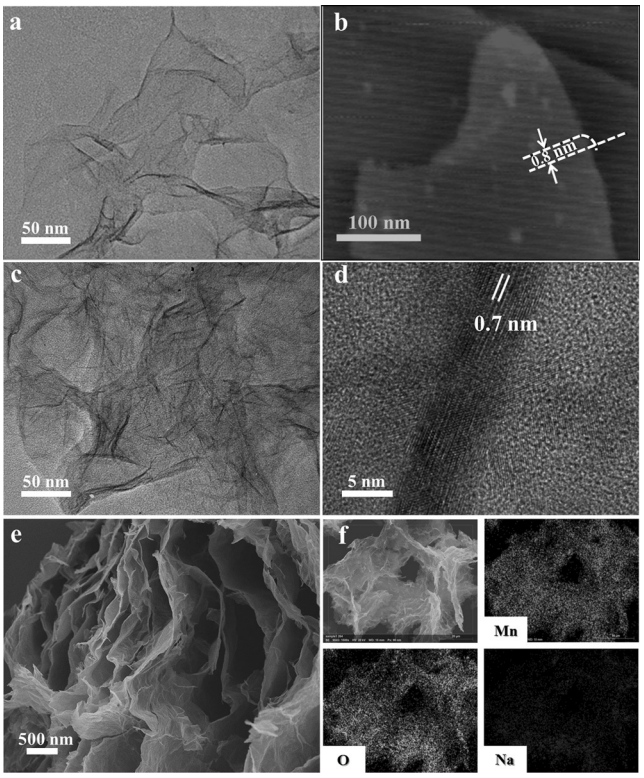

Figure 2. a) TEM and b) AFM images of a manganese oxide nanosheet. c, d) TEM images of NaMO. e) SEM image and f) elemental mapping of NaMO.

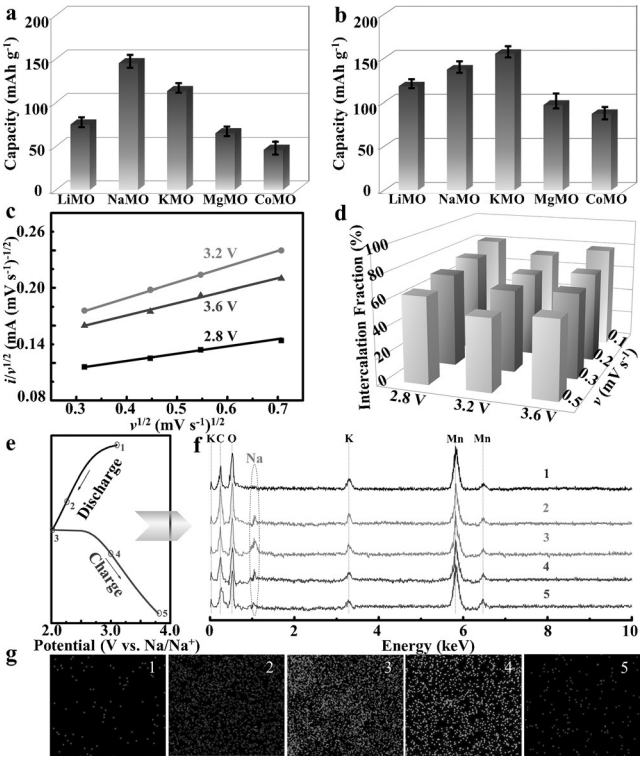

Figure 3. a, b) The specific capacities of M_xMnO_2 for Na (a) and Li (b) storage. The data (average values) correspond to at least three independent assays. c) Plots of $v^{1/2}$ vs. $i/v^{1/2}$ at different potentials; v ($mV s^{-1}$) and i (mA) are the scan rate and current at different potentials, respectively. d) Intercalation capacity contributions under different conditions. e) Discharge and charge curves with the test positions for analysis. f) EDX spectra and g) Na elemental mapping for KMO at different discharge and charge stages in the first cycle.

Na^+ (Figure 2d). The typical lattice spacing is around 0.7 nm, which corresponds to the (001) plane of birnessite-type MnO_2. A scanning electron microscopy (SEM) image (Figure 2e) reveals that the self-assembled NaMO layers are interconnected to form an open, porous three-dimensional structure. Elemental mapping of NaMO confirmed the homogeneous distribution of Na, Mn, and O (Figure 2f). This was corroborated by the EDX spectrum of NaMO (Figure S4), which shows that the sample consists of Mn, O, and Na. The 3D bicontinuous networks of layers and micrometer-sized pores enable both cations (e.g., Li^+, Na^+) and electrons to shuttle easily and reversibly, potentially leading to enhanced performance in Li and Na storage.

The electrochemical performances of the as-prepared M_xMnO_2 samples were initially evaluated by slow-scan voltammetry. The samples exhibited similar behavior for both Li and Na storage owing to the presence of the same manganese oxide sheets (Figure S5). Typically, the broad redox peaks between 2.8 and 2.3 V arise from the large surface with numerous active sites over a wide potential range (Figure S6). However, the manganese oxide nanosheets separated by metal cations with different diameters exhibited different capacities. The discharge capacities of various M_xMnO_2 samples at a current density of $30 mA g^{-1}$ are shown in Figure 3a, b. The corresponding galvanostatic charge–discharge (GCD) profiles (Figures S7 and S8) show obvious discharge plateaus and larger capacities when used as electrode materials for Li storage than when used for Na storage.

The specific capacities of LiMO, NaMO, KMO, MgMO, and CoMO are about 118, 137, 155, 97, and 87 $mA h g^{-1}$ for Li storage and approximately 75, 145, 113, 65, and 46 $mA h g^{-1}$ for Na storage, and thus clearly cation-dependent. MgMO and CoMO, with larger interlayer spacings, gave lower capacities than M_xMnO_2 samples with monovalent cations. To examine the role of hydration, the samples were subjected to a thermal treatment, which resulted in a slight decrease of the interlayer spacing[11] and a decrease of the Na storage capacities (Figure S9), suggesting the supplementary role of water. It has been revealed that the intercalation capacity and the capacitive contribution to energy storage can be quantitatively determined by voltammetry at various scan rates.[13] According to the cyclic voltammograms at various scan rates from 0.1 to 0.5 $mV s^{-1}$ (Figure S10), a good linear relationship (Figure 3c) enables the intercalation capacity contribution to be determined. The calculated capacity contribution from the intercalation is in the range of 59–82% (Figure 3d). The large ratios (>50%) suggest that the energy storage process is dominated by cation intercalation, which was confirmed by the fact that the ratio increased from around 68% to 82% with decreasing the scan rate at a specific potential (2.8 V) as the slow scan rate benefits the intercalation process.

Energy-dispersive X-ray (EDX) spectra of KMO with the corresponding Na elemental mappings at different discharge

and charge stages (Figure 3e) are shown in Figures 3f,g. They reveal the gradual changes in the Na^+ concentration in KMO. During the discharging process, the Na^+ ion concentration gradually increased to reach the maximum value; then, the ions were extracted from KMO in the reverse process, which was also observed by the changes in the Na elemental mapping (Figure 3g). After one charge/discharge cycle, the EDX spectrum of KMO is similar to the original one, suggesting the reversible intercalation/deintercalation of Na^+ ions. The formation of channels through the separation of manganese oxide sheets with cations is crucial for the charge storage process. Further experiments (Figure S11) revealed that the capacity is increased to the maximum value of approximately 145 mA h g^{-1} with an increase in the Na^+/MnO_2 ratio up to 2, but remains constant upon further increasing the ratio. The cation thus likely promotes the formation of channels for Na storage, but an excessive amount of cations does not further enhance the performance.

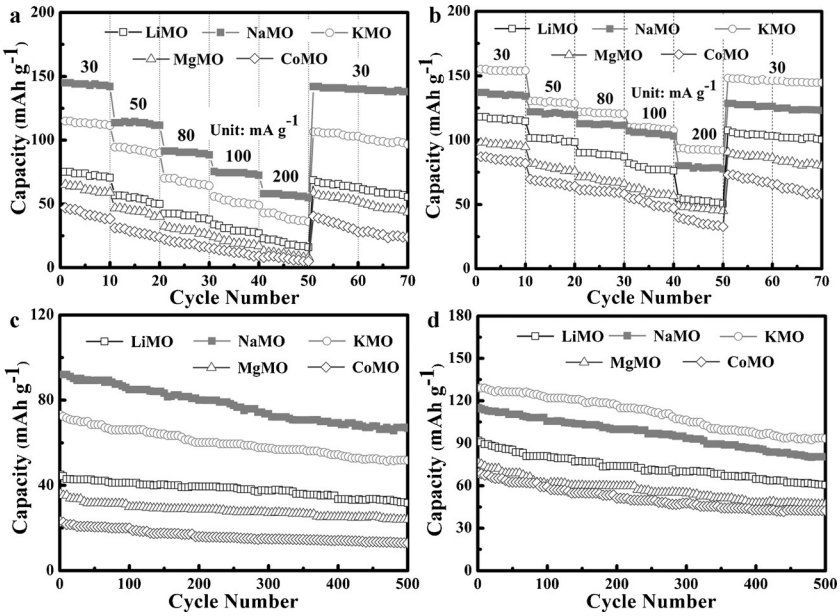

Figure 4. a, b) Rate performance and c, d) cycling stability of M_xMnO_2 for Na (a, c) and Li (b, d) storage.

The above discussion has revealed that the insertion/extraction reactions are the dominating processes. For monovalent guest ions, the discharge capacities follow the order of the ionic diameters and interspaces for Li storage, and KMO exhibited the largest capacity for Li storage of 155 mA h g^{-1}. However, the NaMO cathode contains Na^+ ions in its original framework, which would be more favorable for Na storage in comparison with KMO. Thus, NaMO exhibited the largest capacity for Na storage of 145 mA h g^{-1}. It has been revealed that the interlayer expansion approach is efficient to expand molybdenum disulfide structure for Mg storage.[14] However, CoMO, with a larger interlayer spacing, exhibited smaller capacities for both Li and Na storage than KMO. The capacity of the MgMO electrode was smaller, too. These results show that the interlayer expansion to enhance the capacity is less effective for M_xMnO_2 with divalent cations. Compared with the structures based on monovalent cations, the lower current densities and the smaller discharge capacities of MgMO and CoMO indicate that the insertion of Li^+ and/or Na^+ into the layer space is not facile. The obscure channels that are due to the twisted MnO_2 bilayer (Figure S1) and the Coulomb repulsion forces between the divalent metal ions (e.g., Co^{2+}) and shuttle ions (Li^+, Na^+) potentially result in the lower capacities.[15]

Rate capability tests (Figure 4a,b) revealed that KMO and NaMO exhibit outstanding capacity retention at various rates for both Li and Na storage. When the current density was increased by a factor of approximately 6.7 (30 to 200 mA g^{-1}), the reversible capacity retention of KMO for Li storage was about 61% (155 mA h g^{-1} at 30 mA g^{-1}; 94 mA h at $^{-1}$@200 mA g^{-1}; Figure 4b; vs. 50, 58, 48, and 45% capacity retention for LiMO, NaMO, MgMO, and CoMO, respectively), and KMO hence exhibits the best rate performance. For Na storage (Figure 4a), the capacity retentions of LiMO, NaMO, KMO, MgMO, and CoMO were approximately 32, 40, 38, 21, and 19%, respectively, when the current density was increased from 30 to 200 mA g^{-1}. The rate capabilities of the M_xMnO_2 samples for Na storage are not as good as those for Li storage. According to electrochemical impedance spectroscopy (EIS; Figure S12), the diffusion constant for Li^+ ions in NaMO is 1.8×10^{-12} $cm^2 s^{-1}$, which is larger than that for Na^+ ions (7.5×10^{-13} $cm^2 s^{-1}$). The smaller size and the fast diffusion kinetics may contribute to the better performance in terms of larger capacities and better rate performance for Li storage.[16]

The cycling stabilities of the M_xMnO_2 samples for Li and Na storage are shown in Figure 4c and d, respectively, at a current density of 80 mA g^{-1}. The NaMO electrode maintained approximately 74 and 73% of the initial capacity after 500 cycles for Li and Na storage, respectively. The reversible discharge capacities of LiMO, KMO, MgMO, and CoMO electrodes are about 67, 99, 54, and 45 mA h g^{-1} after 500 cycles for Li storage and approximately 33, 52, 24, and 13 mA h g^{-1} for Na storage, respectively. When used as an anode, LiMO exhibited a specific capacity of 706 mA h g^{-1} at a current density of 100 mA g^{-1} (Figure S13). The discharge capacities and cycling performances of the M_xMnO_2 samples are comparable to previously reported results for Li storage (Table S2).[17] Notably, the use of metal cations with different diameters and valence states in the electrostatic co-precipitation process resulted in different performances for Li and Na storage, and these self-assembled layered M_xMnO_2 electrodes showed cation-dependent capacities and acceptable long-term cycling stabilities for both Li^+ and Na^+ storage.

In conclusion, a bottom-up method has been developed to prepare porous manganese oxide frameworks through the self-assembly of two-dimensional manganese oxide nanosheets separated with various cations (Li, Na, K, Co, and Mg).

The insertion of different cations into the manganese oxide sheets led to a gradual increase in the interlayer spacing, allowing us to improve Li and Na storage. More interestingly, the obtained porous manganese oxide framework pillared with monovalent and divalent cations exhibited different capacities for Li and Na storage. For monovalent cations, the capacity is enhanced by the expansion of the interlayer spacing. The self-assembly of manganese oxide nanosheets with divalent cations (e.g., Co^{2+}) also efficiently broadened the interlayer spacing. However, this did not improve the capacities for Li and Na storage. Thus the experimental results revealed that the capacity and the cycling stability of two-dimensional manganese oxides are influenced by the interlayer spacing and the potential Coulomb repulsion forces between cations. Our results provide a new basis for the rational design of advanced electrode materials by using well-defined 2D metal oxide nanosheets as building blocks.

Acknowledgements

This work was supported by the National Natural Science Foundation of China (21373129 and 21503116).

Keywords: electrochemistry · manganese oxide · nanosheets · sandwich structures · self-assembly

How to cite: *Angew. Chem. Int. Ed.* **2016**, *55*, 10448–10452
Angew. Chem. **2016**, *128*, 10604–10608

[1] a) Y. Sun, Z. Sun, S. Gao, H. Cheng, Q. Liu, J. Piao, T. Yao, C. Wu, S. Hu, S. Wei, Y. Xie, *Nat. Commun.* **2012**, *3*, 1057; b) Z. Sun, T. Liao, Y. Dou, S. M. Hwang, M.-S. Park, L. Jiang, J. H. Kim, S. X. Dou, *Nat. Commun.* **2014**, *5*, 3813; c) J. Hou, Y. Zheng, Y. Su, W. Zhang, T. Hoshide, F. Xia, J. Jie, Q. Li, Z. Zhao, R. Ma, T. Sasaki, F. Geng, *J. Am. Chem. Soc.* **2015**, *137*, 13200–13208.

[2] a) X. Li, X. Ma, D. Su, L. Liu, R. Chisnell, S. P. Ong, H. Chen, A. Toumar, J.-C. Idrobo, Y. Lei, J. Bai, F. Wang, J. W. Lynn, Y. S. Lee, G. Ceder, *Nat. Mater.* **2014**, *13*, 586–592; b) J. R. Kim, G. G. Amatucci, *Chem. Mater.* **2015**, *27*, 2546–2556; c) S.-H. Bo, X. Li, A. J. Toumar, G. Ceder, *Chem. Mater.* **2016**, *28*, 1419–1429.

[3] a) K. Hemalatha, M. Jayakumar, P. Bera, A. S. Prakash, *J. Mater. Chem. A* **2015**, *3*, 20908–20912; b) P.-F. Wang, Y. You, Y.-X. Yin, Y.-S. Wang, L.-J. Wan, L. Gu, Y.-G. Guo, *Angew. Chem. Int. Ed.* **2016**, *55*, 7445–7449; *Angew. Chem.* **2016**, *128*, 7571–7575.

[4] a) M. Nakayama, M. Shamoto, A. Kamimura, *Chem. Mater.* **2010**, *22*, 5887–5894; b) Z. Liu, R. Ma, M. Osada, N. Iyi, Y. Ebina, K. Takada, T. Sasaki, *J. Am. Chem. Soc.* **2006**, *128*, 4872–4880.

[5] a) Z. Liu, K. Xu, H. Sun, S. Yin, *Small* **2015**, *11*, 2182–2191; b) M. Nakayama, S. Konishi, H. Tagashira, K. Ogura, *Langmuir* **2005**, *21*, 354–359; c) J. Qian, H. Jin, B. Chen, M. Lin, W. Lu, W. M. Tang, W. Xiong, L. W. H. Chan, S. P. Lau, J. Yuan, *Angew. Chem. Int. Ed.* **2015**, *54*, 6800–6803; *Angew. Chem.* **2015**, *127*, 6904–6907.

[6] a) C. X. Guo, M. Wang, T. Chen, X. W. Lou, C. M. Li, *Adv. Energy Mater.* **2011**, *1*, 736–741; b) D. Su, H. J. Ahn, G. Wang, *J. Mater. Chem. A* **2013**, *1*, 4845–4850.

[7] a) X. Yang, Y. Makita, Z.-H. Liu, K. Sakane, K. Ooi, *Chem. Mater.* **2004**, *16*, 5581–5588; b) N. Bucher, S. Hartung, A. Nagasubramanian, Y. L. Cheah, H. E. Hoster, S. Madhavi, *ACS Appl. Mater. Interfaces* **2014**, *6*, 8059–8065; c) S. Chen, J. Duan, A. Vasileff, S. Z. Qiao, *Angew. Chem. Int. Ed.* **2016**, *55*, 3804–3808; *Angew. Chem.* **2016**, *128*, 3868–3872.

[8] a) T. Lee, S. H. Min, M. Gu, Y. K. Jung, W. Lee, J. U. Lee, D. G. Seong, B.-S. Kim, *Chem. Mater.* **2015**, *27*, 3785–3796; b) Q. Cheng, T. Yang, Y. Li, M. Li, C. K. Chan, *J. Mater. Chem. A* **2016**, *4*, 6902–6910; c) T. Li, M. Beidaghi, X. Xiao, L. Huang, Z. Hu, W. Sun, X. Chen, Y. Gogotsi, J. Zhou, *Nano Energy* **2016**, *26*, 100–107.

[9] J. Zhang, J. Jiang, X. S. Zhao, *J. Phys. Chem. C* **2011**, *115*, 6448–6454.

[10] a) Y. Omomo, T. Sasaki, L. Zhou, M. Watanabe, *J. Am. Chem. Soc.* **2003**, *125*, 3568–3575; b) Y. Umemura, A. Yamagishi, R. Schoonheydt, A. Persoons, F. D. Schryver, *J. Am. Chem. Soc.* **2002**, *124*, 992–997.

[11] Y. Matsumoto, U. Unal, Y. Kimura, S. Ohashi, K. Izawa, *J. Phys. Chem. B* **2005**, *109*, 12748–12754.

[12] S. Komaba, N. Kumagai, S. Chiba, *Electrochim. Acta* **2000**, *46*, 31–37.

[13] a) T. Brezesinski, J. Wang, S. H. Tolbert, B. Dunn, *Nat. Mater.* **2010**, *9*, 146–151; b) M. Sathiya, A. S. Prakash, K. Ramesha, J.-M. Tarascon, A. K. Shukla, *J. Am. Chem. Soc.* **2011**, *133*, 16291–16299; c) J. Wang, J. Polleux, J. Lim, B. Dunn, *J. Phys. Chem. C* **2007**, *111*, 14925–14931; d) X. Xia, D. Chao, Y. Zhang, J. Zhan, Y. Zhong, X. Wang, Y. Wang, Z. X. Shen, J. Tu, H. J. Fan, *Small* **2016**, *12*, 3048–3058.

[14] Y. Liang, H. D. Yoo, Y. Li, J. Shuai, H. A. Calderon, F. C. R. Hernandez, L. C. Grabow, Y. Yao, *Nano Lett.* **2015**, *15*, 2194–2202.

[15] a) R. Trócoli, F. La Mantia, *ChemSusChem* **2015**, *8*, 481–485; b) K. Lu, B. Song, J. Zhang, H. Ma, *J. Power Sources* **2016**, *321*, 257–263.

[16] a) V. Palomares, P. Serras, I. Villaluenga, K. B. Hueso, J. Carretero-González, T. Rojo, *Energy Environ. Sci.* **2012**, *5*, 5884–5901; b) J. Qian, M. Zhou, Y. Cao, X. Ai, H. Yang, *Adv. Energy Mater.* **2012**, *2*, 410–414.

[17] a) J. Y. Luo, J. J. Zhang, Y. Y. Xia, *Chem. Mater.* **2006**, *18*, 5618–5623; b) F. Jiao, P. G. Bruce, *Adv. Mater.* **2007**, *19*, 657–660; c) L. Li, A.-R. O. Raji, J. M. Tour, *Adv. Mater.* **2013**, *25*, 6298–6302.

Received: May 25, 2016
Revised: June 28, 2016
Published online: July 26, 2016

